Journal of Environmental Management 383 (2025) 125398

Contents lists available at ScienceDirect

Journal of Environmental Management

journal homepage: www.elsevier.com/locate/jenvman

Research article

Deep learning-based spatial optimization of green and cool roof implementation for urban heat mitigation

JiHyun Kim [a,*], Suyeon Choi [a], Mahdi Panahi [a,b,c], Dan Li [d,e], Yeonjoo Kim [a,**]

[a] Department of Civil and Environmental Engineering, Yonsei University, Seoul, Republic of Korea
[b] Department of Physical Geography, Bolin Centre for Climate Research, Stockholm University, Stockholm, Sweden
[c] Department of Sustainable Development, Environmental Science and Engineering (SEED), KTH Royal Institute of Technology, Stockholm, Sweden
[d] Department of Earth and Environment, Boston University, Boston, MA, United States
[e] Department of Mechanical Engineering, Boston University, Boston, MA, United States

ARTICLE INFO

Keywords:
Deep learning-based surrogate model
Pareto optimization
Urban heat mitigation
Cool and green roof
Cost-effectiveness
Heat stress index
Climate change adaptation

ABSTRACT

Intensifying urban heat extremes require efficient mitigation strategies; therefore, we propose a methodological framework for optimizing the implementation of urban green and cool roofs to reduce heat stress while maximizing their cost-effectiveness. In particular, we develop a surrogate model based on the deep learning algorithm Multi-ResNet, which is trained on data generated by the physically-based Weather Research and Forecasting model coupled with an urban canopy model (WRF-UCM). We applied this framework to the Greater Seoul region under the SSP585 climate scenario for 2090–2099 with projected 2100 land cover and evaluated 262,144 scenarios for cool and green roof allocation across 379 urban grids. Our results showed that, at the current cost of green roofs, the Pareto optimal scenario involves implementing cool roofs over 89.2 % of urban areas. This scenario would reduce the total effective heat stress index by 8.8 % compared to the business-as-usual scenario while decreasing costs by 19.6 %. We identified an optimal cost range of 117.4–146.1 $/m over 40 years for green roofs to become cost-effective and more widely adopted. Our approach demonstrates the potential of deep learning techniques to provide efficient quantitative assessments with lower computational demands (from 3561 h with the WRF-UCM to 72 h), potentially supporting climate-resilient urban building planning.

1. Introduction

Urban areas are known to experience unique climatic conditions (Clinton and Gong, 2013; Peng et al., 2012), most notably elevated temperatures, a phenomenon that is referred to as the urban heat island (UHI) effect (Oke, 1973). UHI processes tend to exacerbate heat stress during extreme heat events, with a temperature increase of up to 2.8 °C observed during heat waves (Jiang et al., 2019; Wang et al., 2018). As global climate change accelerates and urban populations continue to grow (Fischer et al., 2021; Northridge and Sclar, 2003), the frequency and severity of urban climatic extremes are projected to increase, threatening public health and raising mortality rates in urban areas (Huang et al., 2019, 2023). To mitigate this impact of extreme heat and the UHI effect, strategic urban planning has become increasingly critical. This often involves the use of physically based numerical modeling, which is employed for preemptive experiments and assessments. For example, the Weather Research and Forecasting (WRF) model (Skamarock et al., 2008) and its variants, coupled with various urban canopy schemes, have been extensively used over the past decade to estimate the effects of cool roofs (CRs) and green roofs (GRs) on a city or regional scale (Georgescu, 2015; Li et al., 2014; Sharma et al., 2016; Wang et al., 2022; Zonato et al., 2021). These numerical assessments have demonstrated that CRs are more effective than GRs in reducing the UHI effect (Georgescu, 2015; Wang et al., 2022; Zonato et al., 2021), though this varies depending on their area (Zhong et al., 2021), and irrigated GRs provide additional cooling effects (Li et al., 2014; Zonato et al., 2021). It has also been suggested that increasing the CR or GR area leads to greater reductions in the UHI effect (Li et al., 2014; Sharma et al., 2016).

In addition to physically based numerical modeling, a growing number of studies have applied machine learning (ML) techniques to develop UHI mitigation strategies. These ML techniques can handle

* Corresponding author.
** Corresponding author.
E-mail addresses: kim.jk237@gmail.com (J. Kim), yeonjoo.kim@yonsei.ac.kr (Y. Kim).

https://doi.org/10.1016/j.jenvman.2025.125398
Received 7 January 2025; Received in revised form 8 April 2025; Accepted 13 April 2025
Available online 23 April 2025

large datasets with numerous variables and capture intricate and nonlinear relationships that may not be fully represented in physically based numerical models. For example, artificial neural networks have been used to provide theoretical guidelines for the optimization of factory designs and the proportion of green space to mitigate extreme UHI effects in Wuhan, China (Liu et al., 2021, 2023). Additionally, Gaussian process regression (Laloy and Jacques, 2019) has been employed to develop a surrogate model for the physically based Arizona State University (ASU) Single-Layer Urban Canopy Model (version 4.1; Li and Wang, 2020), which was subsequently used to determine the optimal urban design parameters (e.g., road width, building height, and albedo) for the mitigation of both urban heat and carbon emissions (Li et al., 2022).

Recent studies have also demonstrated that deep learning (DL) algorithms outperform traditional ML techniques when addressing issues that are inherently complex and spatially heterogeneous with high dimensionality (Johnson and Khoshgoftaar, 2019; LeCun et al., 2015). This advantage is particularly evident in geoscience applications, where DL algorithms enhance seismic data interpretation and advance mineral exploration through the improved analysis of complex geological structures (Yu and Ma, 2021). Similarly, in the energy sector, DL algorithms have been employed to optimize geothermal resource assessment and monitor carbon storage, leading to more precise and efficient modeling (Zhong et al., 2019). Furthermore, in the fields of climate modeling and pollution detection, DL algorithms have substantially increased the accuracy and predictive capabilities of models, enabling more robust environmental analysis and forecasts (Rasp et al., 2018). However, to date, the majority of studies on urban heat mitigation have employed simple ML algorithms to provide uniform optimal parameter values for the entire study region rather than applying DL algorithms to generate spatially heterogeneous urban planning solutions.

In addition to computational techniques used to assess the potential heat reduction that can be achieved through roofing design, comprehensive consideration of costs and benefits is required for the development of sustainable and economically viable urban heat mitigation strategies. For example, while GRs have the potential to reduce building energy consumption by up to 75 % during summer months (Castleton et al., 2010), the expenses associated with their installation, maintenance, and associated stormwater equipment may exceed the benefits gained from energy savings and air pollution removal (Sproul et al., 2014). In particular, it has been estimated that GRs have a net cost of $\$71/m^2$, whereas CRs have the potential to achieve net savings of $\$25/m^2$ (Sproul et al., 2014). Given these economic considerations, it is important to identify optimal roofing strategies that balance financial costs with heat mitigation effects, particularly when considering the implementation of GRs and CRs on a regional scale. However, it is important to note that GRs offer aesthetic, ecological, and recreational benefits that are not easily quantified using existing methods (Manso et al., 2021), while technological advancements in GR implementation may reduce associated costs. Therefore, it is worthwhile to investigate the optimal cost range at which GRs become a viable solution for urban heat mitigation.

In the present study, we developed a DL-based surrogate model to determine optimal roof strategies, including the spatial distribution and

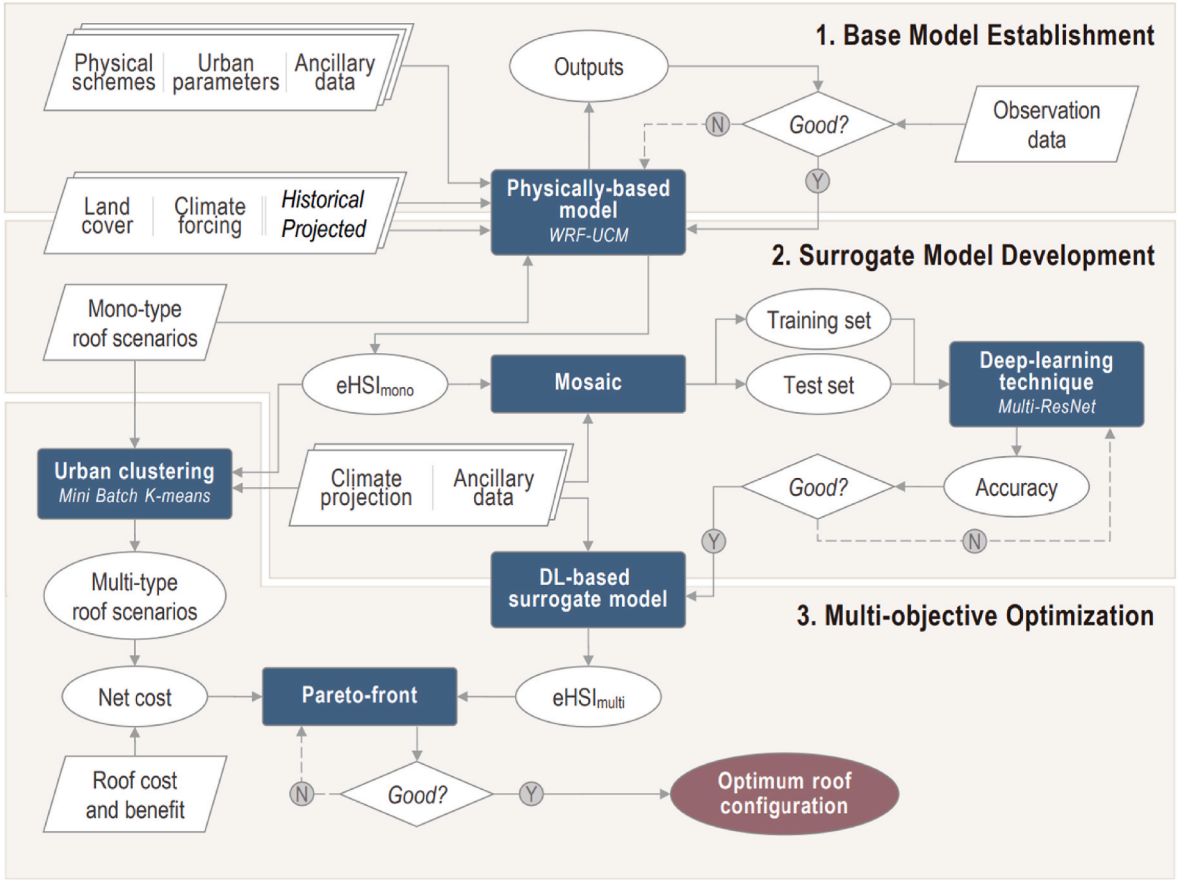

Fig. 1. Workflow for the deep learning-based optimization of the implementation of green and cool roofs for urban heat mitigation. This study involves three main steps. First, the process-based Weather Research and Forecasting model coupled with an urban canopy model (WRF-UCM) was established as the base model. Second, data were generated using the base model, and a surrogate model was developed using the deep-learning Multi-ResNet model (see Fig. 3). Finally, metadata was produced using the surrogate model for multi-type roof scenarios, and the optimal solution was identified based on the trade-off between heat stress mitigation and cost savings.

type (i.e., CRs or GRs), with the objective of maximizing urban heat mitigation while minimizing net costs (Fig. 1). As a case study, we applied this framework to Seoul, the capital of South Korea (Fig. 2) based on its projected climate conditions and land cover changes by the end of this century (2090–2099). We employed the WRF regional climate model coupled with a single-layer urban canopy model (WRF-UCM) to produce the effective heat stress index (eHSI, Eq. (1)) for each of four roof schemes: business-as-usual (BAU), 25 % and 100 % CRs (CR25 and CR100, respectively), and 100 % GR (GR100) (Table S1). After mosaicking the eHSI from each roof scenario (Fig. 3), we trained and tested the DL algorithm Multi-ResNet (Abdi and Nahavandi, 2016) using the mosaicked eHSI along with ancillary data to develop the surrogate model. This DL-based surrogate model was then employed to compute the eHSI for 262,144 multi-type roof scenarios. The optimal roof scenarios at the current GR cost were determined using Pareto optimization (Ngatchou et al., 2005), which identifies a set of solutions where no objective can be improved without compromising another, thus providing a balanced trade-off between the total eHSI and total cost. We then estimated the optimal cost range for GRs that would enable coverage of more than half of the urban area. This framework represents a state-of-the-art tool that integrates physically based models, DL techniques, and multi-objective optimization for use in the development of urban heat mitigation strategies that address the complexity of urban heat stress under future climate scenarios.

2. Methods

2.1. Study region

The study region included Seoul and its surrounding areas (36.4896–38.207 °N, 126.0979–128.0743 °E), covering a population of 26 million as of 2023 (https://kosis.kr/) (Fig. 2b). With a land area of 2.4 Mha, the study region during the 2000–2004 period consisted of urban areas (4.7 %, including low and high-intensity residential areas and commercial areas), forests (56.9 %, including deciduous, evergreen, and mixed forests), and other land cover (including croplands, grasslands, and wetlands) (https://egis.me.go.kr). The annual mean temperature and precipitation in the study region from 2000 to 2021 were 12.4 °C and 1286.6 mm, respectively (https://data.kma.go.kr/).

2.2. Base model: WRF-UCM

As the base model, we employed the WRF with the Advanced Research WRF dynamic core (WRF-ARW) regional climate model (version 4.3.3; Skamarock et al., 2021), coupled with a single-layer UCM (Kusaka et al., 2001; Kusaka and Kimura, 2004). Key urban processes, such as shadowing, reflections, and the trapping of radiation and energy in the urban canyon via roofs, walls, and roads, are represented in the UCM. Therefore, the WRF-UCM has been widely used to investigate the effects of climate change and anthropogenic activities in urban areas (Vahmani and Hogue, 2015; Wang et al., 2022).

We established three two-way nested grids with spatial resolutions of 27 km, 9 km, and 3 km (number of grids = 100 × 103, 82 × 91, and 51 × 60, respectively), with the innermost domain centered over Seoul and the surrounding suburban areas (Fig. 2). The vertical grids were set to have 45 levels, with the top level at 50 hPa. The physical parameterization schemes were as follows: the WRF Single-Moment 3-Class (WSM3) microphysics scheme (Hong et al., 2004), the Rapid Radiative Transfer Model (RRTM) for long- and short-wave radiation schemes (Mlawer et al., 1997), the revised MM5 surface layer scheme (Jiménez et al., 2012), Noah-LSM (Tewari et al., 2004) for land surface processes, the Yonsei University planetary boundary layer scheme (YSU) (Hong et al., 2006), the Kain–Fritsch cumulus scheme (Kain and Fritsch, 1990) with no cumulus parameterization for domain 3, and the UCM (Kusaka et al., 2001; Kusaka and Kimura, 2004) for urban surface processes.

We generated two land cover maps at a resolution of 3 km: a historical map to evaluate the WRF-UCM and a future map to assess the effects of the roof scenarios. The historical map was generated by rescaling the level-2 map from the Ministry of Environment of South Korea, https://egis.me.go.kr, 5-m resolution) and then reclassifying it following the U.S. Geological Survey (USGS) 24 land cover classification categories with three urban categories (low and high-intensity residential areas and commercial areas) (Fig. 2b). The future map was taken from the land cover change scenario for 2100 under the SSP585 scenario (Chae et al., 2017), which we reclassified following the USGS 24 land cover classification categories (Fig. 2c). Urban parameters for the urban grids are summarized in Table S2.

For the initial and boundary conditions, we used a global dataset (horizontal grid spacing of 1.25° × 1.25° at 6-h intervals for the 1979–2100 period) based on the mean climate and interannual variance of the European Centre for Medium-Range Weather Forecasts Reanalysis 5 (ERA5), the bias of which was corrected using a nonlinear trend from

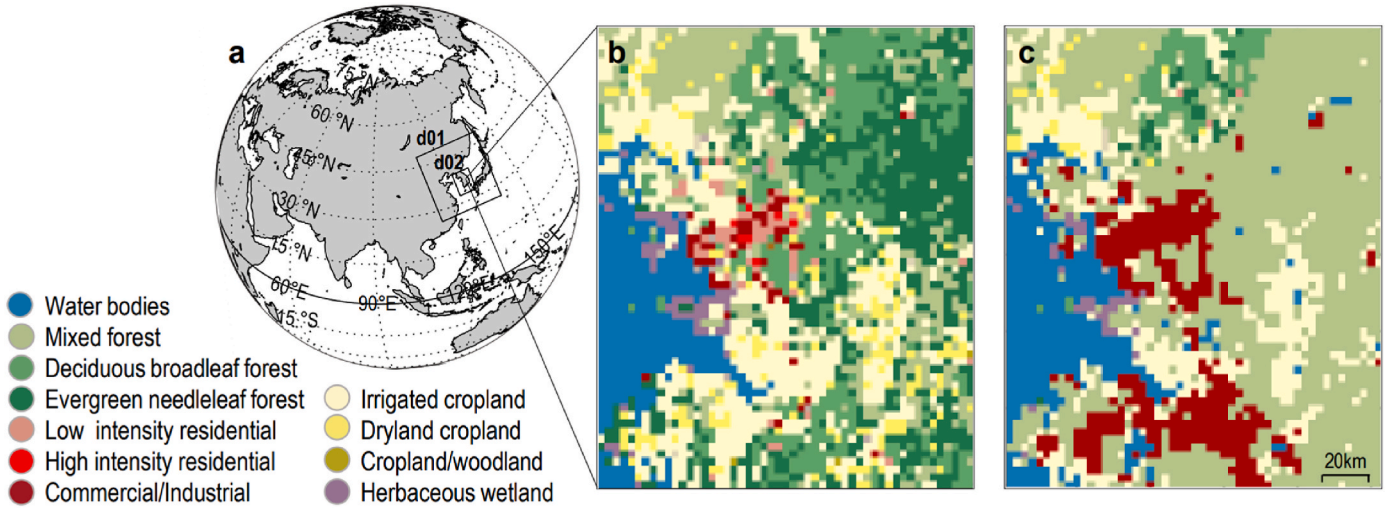

Fig. 2. Study region. (a) Weather Research and Forecasting model coupled with an urban canopy model (WRF-UCM) applied to three nested domains: d01 (23.2431–50.8376 °N, 109.363–147.6499 °E), d02 (31.7593–39.9859 °N, 122.6212–131.9247 °E), and d03 (36.4896–38.207 °N, 126.0979–128.0743 °E). (b) Study region (d03) encompassing Seoul and its surroundings, with land cover data for 2000–2004 obtained from the Environmental Geographic Information Service (https://egis.me.go.kr). (c) Projected land cover map for the year 2100 generated based on the Shared Socioeconomic Pathway 585 (SSP585) scenario[1].

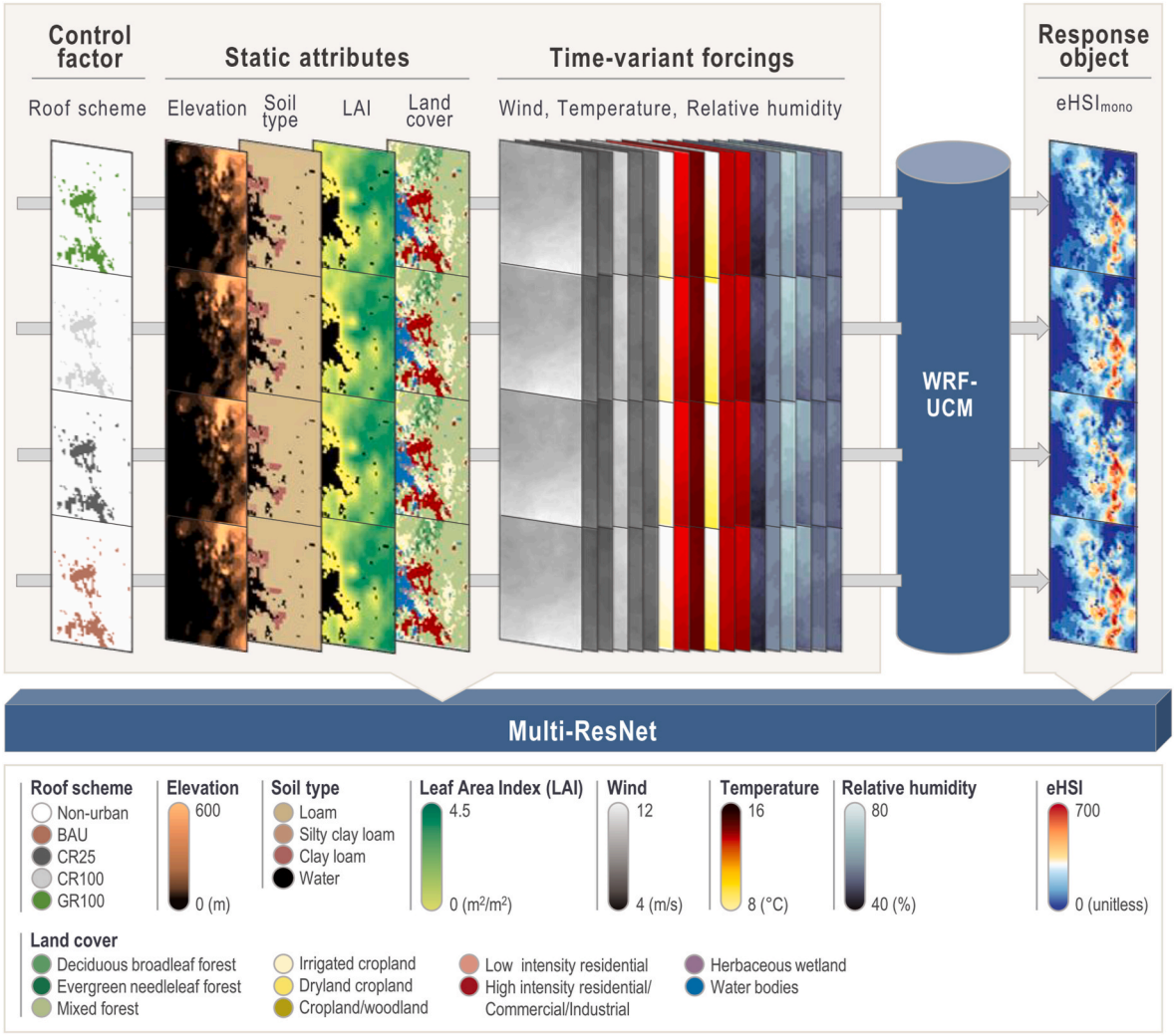

Fig. 3. Schematic diagram of the sample data generation and mosaic process. The Weather Research and Forecasting model coupled with an urban canopy model (WRF-UCM) was employed to generate sample data to calculate the total effective heat stress index (eHSI) for four mono-type roof scenarios: business-as-usual (BAU), 25 % cool roofs (CR25), 100 % cool roofs (CR100), and 100 % green roofs (GR100) (Table S1). To construct training and testing datasets for the Multi-ResNet model, we mosaicked the roof schemes, ancillary datasets, time-variant forcings, and the response variable (i.e., $eHSI_{mono}$ from the WRF-UCM). The ancillary datasets were static attributes (elevation, soil type, leaf area index, and projected land cover), which were replicated four times. Time-variant forcings (temperature, relative humidity, and wind) were monthly averages from June to August over two five-year periods (2090–2094 and 2095–2099). The $eHSI_{mono}$ values represented the 10-year averages for each roof scheme and meteorological forcing set.

the ensemble mean of 18 Coupled Model Intercomparison Project Phase 6 (CMIP6) models (Xu et al., 2021) (Table S3). The simulation period covered the summer season from June to August (JJA), when heat stress is strongest within the study region. The model was initialized on 1 May with a one-month spin-up for each simulation year during the model evaluation period (2000–2009) and the future scenario period (2090–2099). We evaluated the model performance based on the Pearson correlation coefficient (r) and the root-mean-squared error (RMSE) for the comparison between the simulation results (2-m air temperature, relative humidity, and precipitation) and the measurement data at five meteorological stations from the National Climate Data Portal of the Korea Meteorological Administration (http://data.kma.go.kr) during the historical period (i.e., JJA of 2000–2009).

2.3. Sample data generation

Using the WRF-UCM with the future SSP585 climate scenario and a land cover scenario for 2100 (Chae et al., 2017) (Fig. 2c), we generated a sample dataset by setting all of the roofs in the urban grids as a mono-type roof scheme for the four options: BAU, CR25, CR100, and GR100 (Table S1). For each roof scheme, the albedo parameter for the urban grids was set to the value representing each roof type. For the GR100 scheme, the GR option in the WRF-UCM model was employed instead of altering the albedo.

We calculated the objective variable HSI (Ha et al., 2022; Rothfusz, 1990) using simulated 3-h outputs (temperature, water vapor mixing ratio, and surface pressure) with each mono-type roof scheme (HSI_{mono}). Because an HSI higher than 105 is considered to represent extreme caution or even danger (Ha et al., 2022), we added together the HSI_{mono} exceeding this threshold during JJA each year to produce the eHSI ($eHSI_{mono}$, Eq. (1)).

$$eHSI_{mono} = \sum_{h=1}^{N} \left(HSI_{mono,h} - \theta_{HSI} \right) \quad \text{(Eq. 1)}$$

where $HSI_{mono,h}$ indicates the 3-h HSI for the roof scheme, θ_{HSI} is the threshold (105), and N is the number of data points (i.e., 736 over the three months).

2.4. Deep learning model: Multi-ResNet

Multi-ResNet (Abdi and Nahavandi, 2016) was employed as the surrogate model in this study. This selection was based on its proficiency in processing high-dimensional data with spatial heterogeneity (LeCun et al., 2015), making it particularly suitable for handling complex datasets derived from WRF-UCM outputs. Multi-ResNet extends the concept of ResNet by introducing multiple residual functions in each block (MultiResBlock, Fig. S1, Table S4) in parallel or in a hierarchical manner with varying kernel sizes (e.g., 1 × 1, 3× 3, 5× 5, and 7× 7) to capture different levels of features or representations from the input data, such as urban grid attributes and meteorological forcings. These features are integrated through concatenation, batch normalization, and ReLU activation to integrate and refine features across scales, with residual connections ensuring robust gradient flow through the network. The architecture progressively reduces the spatial dimensions while deepening the feature representations through successive blocks. It then employs global average pooling to aggregate spatial information and fully connected layers for the prediction of the output (eHSI in this study). This structure facilitates the efficient and accurate modeling of complex urban heat mitigation scenarios.

In this study, the hyperparameters of Multi-ResNet were optimized using grid search method to enhance its urban heat stress prediction performance. In particular, a learning rate of 0.001, the Adam optimizer, a batch size of 32, training over 200 epochs, and seven MultiResBlocks were employed (Fig. S1). A dropout rate of 0.3 was used to prevent overfitting, while ReLU activation with batch normalization was employed within each MultiResBlock to capture multi-scale features from the urban grid data and meteorological forcings, ensuring the accurate prediction of the eHSI across multiple roof scenarios.

To train and test a single Multi-ResNet with the four mono-type roof scenarios simultaneously, we generated mosaic sets of both the input data (i.e., the roof schemes, static attributes, and time-variant meteorological forcings) and output data (i.e., eHSI) (Fig. 3). The mosaic for the roof schemes was created by aligning BAU, CR25, CR100, and GR100. Static attributes (e.g., elevation, soil type, leaf area index, and future land cover map) were duplicated four times. Each time-variant meteorological forcing variable (e.g., monthly median temperature, relative humidity, and wind) was averaged over two five-year periods (2090–2094 and 2095–2099) and then duplicated. As a result, two mosaic sets were produced for each variable each month: the first set corresponding to the years 2090–2094 and the second set corresponding to the years 2095–2099. The $eHSI_{mono}$ derived from WRF-UCM was averaged for the 2090–2099 period for each mono-type roof scheme. We then aligned these four $eHSI_{mono}$ values with the order of the roof schemes in the mosaic. The 12,240 grids in the mosaic sets (51 × 60 grids in the domain with the four roof schemes) were divided into two groups, with 70 % of the grids used for training over 200 epochs and 30 % used for testing (Ghorbanzadeh et al., 2022). During the training process, 10 % of the data was used for validation to avoid overfitting (Srivastava et al., 2014).

The performance of Multi-ResNet was assessed based on its accuracy (ACC) and average F1-score derived from the testing data (Eqs. (3) and (4), respectively):

$$ACC = (TP + TN)/(P + N) \quad \text{(Eq. 3)}$$

$$F1 = 2 \times \left[(precision \times recall)/(precision + recall)\right] \quad \text{(Eq. 4)}$$

where TP and TN represent true positives and true negatives (i.e., correctly predicted positive and negative classes, respectively), while P and N are the actual positive and negative classes, respectively. We also evaluated Multi-ResNet based on r and RMSE to allow a comparison between the eHSI predictions from Multi-ResNet and those from the WRF-UCM for the four mono-type roof scenarios (i.e., BAU, CR25, CR100, and GR100). After validating its performance, Multi-ResNet was employed as the surrogate model for the simulation of the eHSI under the multi-type roof scenarios.

2.5. Urban grid clustering

The mini-batch K-means method is a variant of the widely used K-means method (Lloyd, 1982), which has some disadvantages, such as its sensitivity to initial centers, outliers, and the number of clusters (Sculley, 2010). Mini-batch K-means clustering assigns the dataset to small random batches with a fixed size and calculates the centroid in each batch. New batch assignments and centroid calculations are iterated until convergence or a preset number of iterations is reached (100 in the present study).

For clustering purposes, we normalized nine variables related to three attributes of urban grids: geospatial information (i.e., latitude and longitude), background climate forcings (i.e., median temperature, relative humidity, and wind speed for the 2090–2099 period), and the response variable (i.e., mean $eHSI_{mono}$ for BAU, CR25, CR100, and GR100 during the 2090–2099 period).

We calculated cost function J (Eq. (5)) while increasing the number of clusters ($N_c = 0 \ldots 10$) and selected the optimal number of clusters (N_{opt}) using the elbow method (Nainggolan et al., 2019; Syakur et al., 2018), which identifies the point around which changes in the cost function decrease rapidly.

$$J_{N_c} = \sum_{c=1}^{N_c} \sum_{d=1}^{N_d} \sum_{a=1}^{N_a} \left| x_{c,d,a} - C_{c,a} \right|^2 \quad \text{(Eq. 5)}$$

where J_{N_c} is the cost function with the cluster number (N_c), N_d is the number of data points in cluster c, N_a is the number of the attributes considered (nine in this study), $x_{c,d,a}$ is the normalized value of the data point in cluster c with attribute a, and $C_{c,a}$ is the center value of cluster c with attribute a.

2.6. Metadata generation and Pareto optimization

Once the optimal number of clusters of urban grids (N_{opt}) was determined, we produced multi-type roof scenario maps by assigning one roof scheme to one cluster and changing the roof schemes in a sequential manner, resulting in a total of $4^{N_{opt}}$ multi-type roof scenarios. We implemented the surrogate Multi-ResNet model for each roof scenario with the other input data (i.e., future climate projections and ancillary data), generating $eHSI_{multi}$. The economic net cost of each roof scheme over 40 years was calculated as the sum of costs (e.g., installation and maintenance) minus the sum of the benefits (e.g., avoided CO_2, NO_x, and SO_2 emissions) after considering inflation and discount rates (Table S5), and the total cost was calculated by multiplying the net cost with the area of the roof scheme.

To identify the optimal roof scenarios that provided a balance between the reduction in the heat stress and the total cost, we searched for Pareto solutions (Ngatchou et al., 2005) from the $4^{N_{opt}}$ scenarios where $eHSI_{multi}$ could not be reduced further without increasing the total cost. In this study, we opted for Pareto optimization due to its superior efficiency in identifying non-dominated solution sets. This approach offers distinct advantages over alternative methods, such as the weighted-sum technique, which requires the arbitrary assignment of weights to various objectives, and multi-objective evolutionary algorithms, which are computationally intensive (Gunantara, 2018). Both $eHSI_{multi}$ and the total cost were normalized prior to searching for the Pareto solutions. We also identified the optimal roof scenarios under the assumption that the GR cost would continue to decrease. The Pareto solutions were assessed as the net cost of the GR scheme decreased in increments of $1 from the current cost. We then proposed an optimal cost range for the GR scheme that would enable coverage of more than half of the urban areas, making it the optimal scenario for heat reduction and cost savings.

3. Results and discussion

3.1. Surrogate model development

The performance of WRF-UCM, the physically based model used to generate data for the surrogate model, was evaluated using measurements at five meteorological stations (Table S6). The Pearson correlation coefficient (r) was 0.75–0.86 for the 2-m air temperature, 0.56–0.83 for the 2-m relative humidity, and 0.55–0.61 for precipitation, while the RMSE was within an acceptable range (1.2–1.5 °C, 41.1–183.4 mm, and 7.2–10.0 %, respectively). These metrics were comparable to previous studies (Ding and Chen, 2024; Du et al., 2022; Wang et al., 2017), indicating a reasonable consistency between model simulations and measurements.

Using Multi-ResNet, the accuracy of both the training and validation groups gradually converged after approximately 100 epochs (Fig. S2). The overall accuracy (0.84) indicated that 84 % of the model predictions were correct, while the F1-score (0.84) suggested that the model reliably identified high eHSI values despite their rarity, thus it could handle an imbalanced dataset. Similarly, r and RMSE were 0.73 and 53.5 (approximately 10 % of the maximum eHSI), respectively, supporting the reliability of Multi-ResNet as a surrogate model for the roof scenario simulations.

3.2. Metadata analysis and optimal scenarios

Running simulations for all four roof schemes (i.e., CR25, CR100, GR100, and BAU) on each of the urban grids ($N = 379$) would require the analysis of 4^{379} scenarios (about $1.52 \times 10,^{228}$), which is prohibitive in terms of computing power and time. Therefore, to reduce the total number of scenarios, we clustered the urban grids using the mini-batch K-means method (Chavan et al., 2015; Sculley, 2010). Based on the peak curvature for the cost function (J) (Fig. 4a), the optimal number of urban clusters was determined to be nine, where there was a steep decline in the rate of change of the cost function ($N_{opt} = 9$, Fig. 4a). This optimal cluster number represents an ideal balance between maximizing computational efficiency (achieved through fewer clusters) and model performance (minimizing within-cluster variance). The smallest cluster (#3) consisted of 16 grids scattered across the northeastern area, while the largest cluster (#4) included 70 grids and was located in the mid-western region (Fig. 4b). Each of the four roof schemes was systematically applied to each of the nine clusters, starting with a baseline scenario where the BAU scheme was applied to all clusters. In subsequent scenarios, other roof schemes (i.e., CR25, CR100, and GR100) were applied to individual clusters while maintaining BAU for the others. This systematic variation continued, exploring all possible combinations of roof schemes across the clusters, generating a total of 262,144 unique scenarios (i.e., 4^9; see the four examples in Fig. S3).

We found that there was considerable variation in the total eHSI derived from the surrogate model across these roof scenarios (Fig. 5a). This indicated that there is significant potential for heat stress mitigation within the study region by implementing appropriate roof schemes in the designated areas. Notably, when applied across all urban areas, the GR100 scheme led to the largest reduction in heat stress, with a 15.8 % decrease in the total eHSI compared to the BAU scheme. Similarly, the total costs associated with each of the roof scenarios varied substantially. Implementing the GR100 scheme across all urban areas generated the highest cost ($339.6 billion), 43.5 % higher than the total cost of the BAU scheme ($236.7 billion), while the scenarios associated with the CR100 scheme generated the lowest total cost ($190.2 billion). The majority of the roof scenarios were characterized by an inverse relationship between total cost and heat stress, with higher costs leading to a stronger mitigation effect. Overall, the considerable differences in the total eHSI and total cost highlight the importance of considering both environmental and economic factors when developing urban heat mitigation strategies.

Our analysis of 262,144 scenarios yielded 46 Pareto solutions that balanced a reduction in heat stress with a reduction in cost (Fig. 5b). The

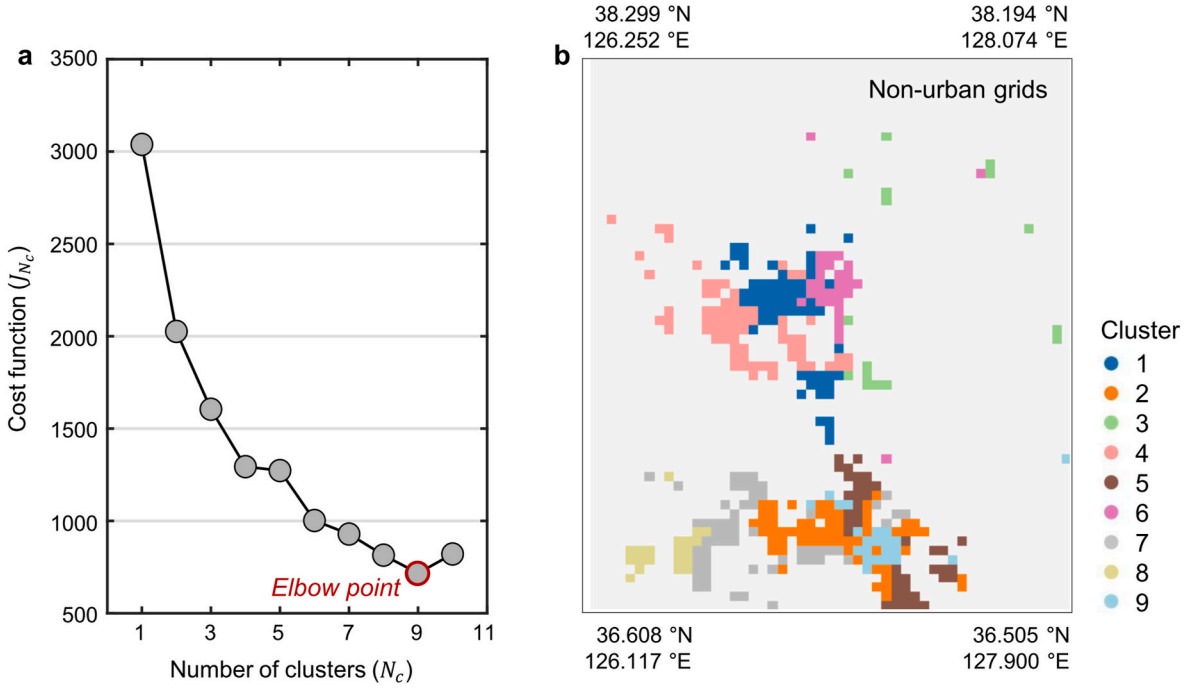

Fig. 4. Clustering urban grids. (a) Cost function (J, Eq. (5)) for varying cluster numbers (N_c) using the mini-batch K-means method (gray circles). The clustering process incorporated nine variables across three attributes: geospatial information (latitude and longitude), climate forcings (average temperature, relative humidity, and wind speed for the period 2090–2099), and response variables (mean eHSI under the BAU, CR25, CR100, and GR100 roof scenarios for 2090–2099 from the WRF-UCM). The optimal number of clusters (nine) was determined as the elbow point (red open circle), where the rate of change of the cost function decreases notably. (b) Spatial distribution of the resulting nine clusters across the 379 urban grids.

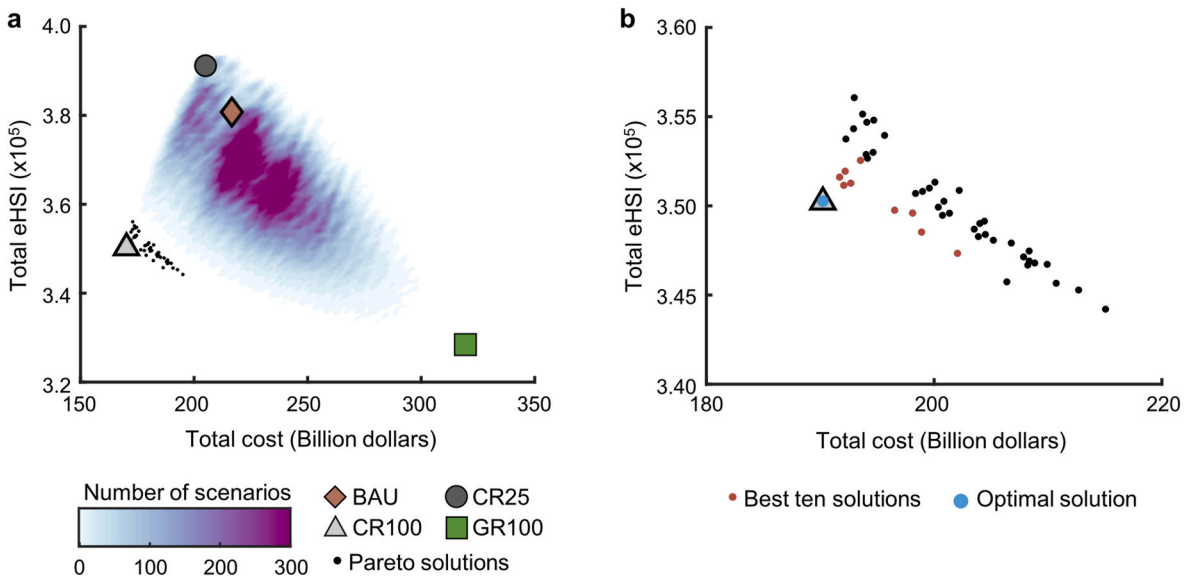

Fig. 5. Pareto-optimal solutions. (a) Density plot of the number of scenarios according to their total effective heat stress index (eHSI) and associated total costs. The mono-type roof scenarios are business-as-usual (BAU; brown diamonds); 25 % cool roofs (CR25; dark-gray circles); 100 % cool roofs (CR100; light-gray triangles); and 100 % green roofs (GR100; green squares). The 46 Pareto-optimal solutions are indicated by black dots. (b) All Pareto solutions (black dots) together with the ten best solutions (red dots) and the optimal solution (blue dot).

optimal scenario was identified to be implementing the CR100 scheme across all of the urban areas (Figs. 5b and 6a). This scenario reduced costs by 19.6 % compared to the BAU scheme, while reducing heat stress by 8.8 %. The eHSI with the optimal scenario was significantly different from that with BAU and GR100 ($p < 0.001$, Fig. S4), indicating a significant effect of the roof implementations on heat reduction. The next nine best-performing Pareto solutions exhibited a consistent pattern, with the CR100 scheme dominating the spatial configurations and the other roof schemes (GR100, CR25, and BAU) making up only 4.2–10.8 % of the total urban area (Fig. 6b). These results also demonstrated that the implementation of uniform roof schemes produced spatially heterogeneous effects on urban heat stress (Fig. 6c). Specifically, the heat stress reduction was minimal for the CR100 scheme in dispersed and isolated regions, with little change in the eHSI compared to the BAU scheme. In contrast, the largest heat stress reduction was observed in central urban areas. These heterogeneous effects can be attributed to the complex interactions between various factors, including local microclimates and urban morphology, highlighting the need for a robust framework capable of comprehensive analysis. Our analysis also suggested that tangible mitigation requires not only sufficient area coverage of the implemented roof schemes but also an adequate concentration of these strategies within the urban landscape. Adopting a uniform roof scheme across the entire city may not be sufficient to ensure effective heat stress reduction, meaning that a spatially targeted approach to urban heat mitigation is required.

3.3. Optimal GR cost range and efficacy of the roofing strategy

The current net cost of GRs is 209.6 $/m^2 for a 40-year period (Table S5), which means that they could only be implemented over a limited proportion of the urban areas (4.2–10.8 %) in the Pareto solutions (Fig. 6b). In order for GRs to be a viable solution for urban heat stress mitigation, by which they should cover more than half of the urban areas, their net cost needs to be lower. To explore the impact of potential reductions in GR costs, we analyzed the Pareto solutions for all roof scenarios with GR costs ranging from the current net cost to a lower bound of 100 $/m^2 over a 40-year period (Fig. S5 and Fig. 7a). Our results indicated that, when the costs of GRs exceeded that of the BAU scheme (146.1 $/m^2 over a 40-year period), increasing the GR area led to an almost linear increase in total costs (Fig. 7b). It was also observed that the total eHSI could not be reduced below a certain threshold (3.43×10^5), indicating that the heat mitigation efficacy was limited within this range of GR costs (Fig. 7c). Once the GR costs fell below that of BAU, a large increase in the GR area was observed in the Pareto solutions. This was accompanied by a noticeable reduction in the total eHSI without large increases in total costs (Fig. 7a–c). In addition, when the GR costs were lower than that of the CR100 scheme (117.4 $/m^2 over a 40-year period), the scenario in which the GR100 scheme was employed across all urban areas emerged as the sole optimal solution. This non-linear pattern in the total eHSI and GR area in relation to the GR costs could be used to determine the optimal cost range for GRs, within which the cost-effectiveness of its implementation substantially improved. These results collectively suggest that achieving specific cost thresholds for GRs could facilitate their widespread adoption without proportional increases in total costs.

In addition to the consideration of overall coverage and cost, the spatial configuration of roof schemes is also a critical factor in optimizing urban heat mitigation. We thus compared two roof scenarios with contrasting spatial distributions but identical compositions: 50 % of GR100 and 50 % of either CR100 or CR25 (Fig. 8a–d). This revealed differential heat mitigation effects across the urban landscape (Fig. 8e–j), highlighting the potential for stronger mitigation in specific areas or diffuse cooling effects across larger urban expanses without increasing the overall implementation costs. This variability illustrates the importance of optimizing not only the extent but also the spatial configuration of roof schemes to enhance urban heat mitigation benefits. Our findings indicate that robust processes for implementing roof strategies that are optimized to the specific climatic and economic characteristics of urban environments need to be developed.

3.4. Study limitations and future research directions

We propose a methodological framework for determining the optimal distribution of CRs and GRs for urban heat mitigation, yet it is important to acknowledge its limitations. First, our analysis was confined to a single city, which may limit the generalizability of our framework to other cities with different urban morphologies and climatic characteristics. In addition, the use of a single climate scenario

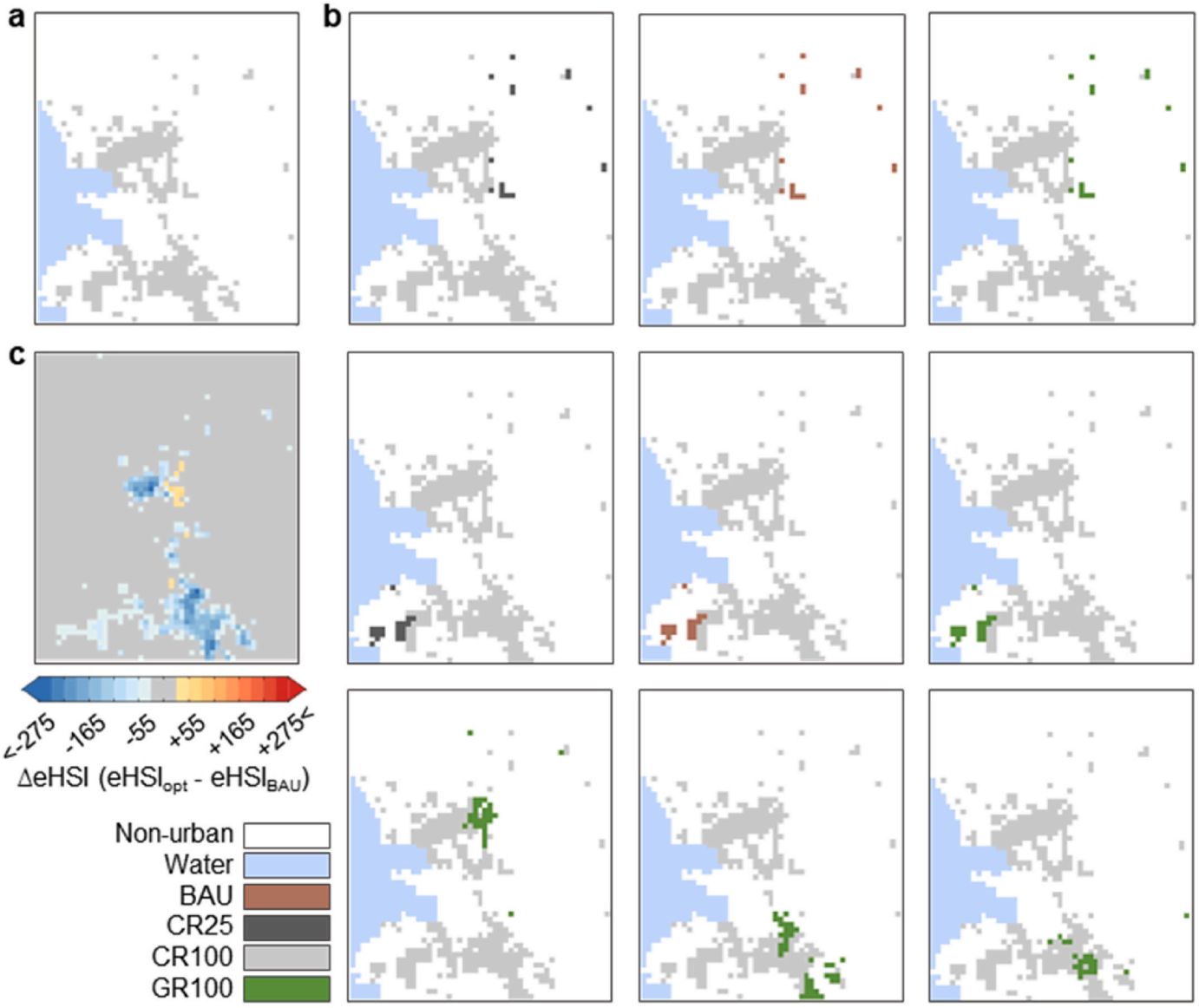

Fig. 6. Pareto-optimal roof configurations and associated heat stress reduction. (a) Optimal solution for heat stress mitigation that also balances cost, which predominantly implements the 100 % cool roof (CR100) scheme (in white) across the urban areas. (b) For the next nine best Pareto solutions, the CR100 scheme is consistently preferred, with alternative schemes (business-as-usual [BAU], 25 % and 100 % cool roofs [CR25 and CR100], and 100 % green roofs [GR100], Table S1) used in 4.2–10.8 % of the urban areas. (c) Difference in the total effective heat stress index (eHSI) between the optimal solution and the BAU scheme, highlighting the effectiveness of this configuration in reducing heat stress.

(SSP585) may limit the robustness of long-term heat mitigation strategies, given the inherent uncertainties in future climate projections. Therefore, future research should extend this approach to multiple cities across a diverse range of climate regimes and projections to validate the applicability of the model and investigate the efficacy of CRs and GRs for heat mitigation.

Our framework also has a predominantly environmental and climatic focus when developing the DL-based surrogate model. The effectiveness of heat mitigation strategies may vary considerably based on socioeconomic factors such as population density, resident activity patterns, the use of cooling systems, and local economic conditions. For example, areas with a higher socioeconomic status may have better access to air conditioning, whereas lower-income communities may rely more on passive cooling strategies, such as shaded outdoor spaces and natural ventilation (Li et al., 2024). However, those communities may struggle to maintain green infrastructure, potentially reducing its long-term cooling effectiveness (Schwarz et al., 2015). Understanding these complex feedback loops involving environmental parameters and socioeconomic factors is essential for tailoring mitigation strategies that address the needs of various populations. Therefore, by incorporating socioeconomic datasets such as census data, land-use surveys, and behavioral studies, future research can improve the effectiveness of strategies designed to mitigate future heat risks.

Another issue may arise from the clustering approach in this study, which grouped 379 urban grids into nine clusters. This approach aimed to provide a degree of localization to reduce the computational requirements, but it may fail to generate completely localized recommendations across urban grids. Even though climate variables (i.e., temperature, relative humidity, and wind speed) were employed during clustering, intra-cluster microclimate variation may have affected the accuracy of the optimal CR and GR distribution strategies, potentially leading to suboptimal mitigation outcomes. While clustering provides a practical framework for city-scale analysis, it may oversimplify the localized recommendations needed for effective heat mitigation at the

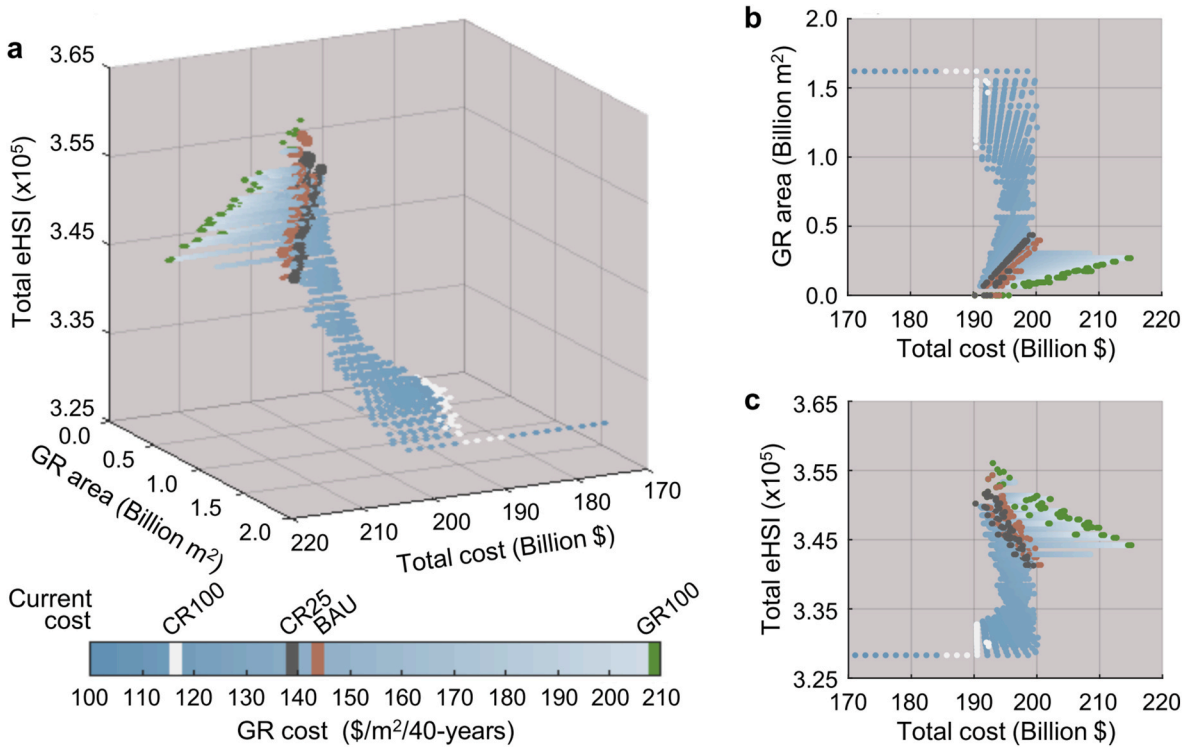

Fig. 7. Pareto-optimal solutions for varying green roof (GR) costs. (a) Distribution of the total effective heat stress index (eHSI), total costs, and GR areas for the Pareto-optimal solutions that balance the total eHSI and total costs for a range of GR costs from the current value (209.6 $/m^2 over a 40-year period, Table S5) to 100.0 $/m^2 over a 40-year period. The current costs of each roof scheme (i.e., business-as-usual [BAU], 25 % and 100 % cool roofs [CR25 and CR100], and 100 % green roofs [GR100]; Table S5) are colored accordingly. (b) Distribution of GR areas according to the associated total cost. (c) Distribution of the total eHSI in accordance with the associated total cost.

neighborhood scale. Future research should consider employing higher-resolution data and more advanced clustering techniques to better capture the heterogeneity of urban environments and provide more localized, effective recommendations for heat mitigation strategies.

Another potential concern is that the economic analysis in this study employed certain simplifications that may limit its applicability to real-world decision-making. Specifically, it does not account for regional variation in installation and maintenance costs, which can influence the feasibility of heat mitigation strategies. In addition, the non-monetary benefits of GRs, such as improved air quality, enhanced stormwater management capacity, and improved biodiversity, were not included in the cost estimation, despite their substantial contribution to the overall urban environment. Another limitation is the simplified net cost estimations over the 40-year period, which only considered inflation and discount rates but not technological advancements or economies of scale. Future research should incorporate dynamic cost models and broader cost–benefit frameworks to capture the full economic benefits of these strategies.

4. Conclusion

The use of CRs or GRs is effective in mitigating urban heat (Berardi et al., 2014; Rawat and Singh, 2022). In this study, we proposed a framework for the optimization of the CR and GR distribution to mitigate urban heat while simultaneously considering economic costs. Using a Multi-ResNet-based surrogate model trained on the eHSI from the physically based model WRF-UCM, we found that the implementation of the CR100 scheme across the majority of urban areas achieved the optimal balance of heat stress reduction (8.8 %) and cost savings (19.6 %) compared to the BAU scenario in the Greater Seoul region under the SSP585 climate scenario during the 2090–2099 period. We also identified an optimal cost range for GRs of 117.4–146.1 $/m^2 over a 40-year period, making GR implementation substantially more viable without a proportional increase in overall costs. Our findings demonstrate the importance of spatial configuration considerations because the roof schemes exhibited heterogeneous effects on heat stress mitigation across different urban areas, highlighting the need for spatially targeted approaches.

Despite potential limitations discussed above, our study demonstrates the value of surrogate modeling in efficiently exploring a large number of scenarios, allowing for more informed decision-making in urban planning. In particular, the surrogate model significantly reduced the computing time to approximately 72 h for 262,144 scenarios, compared to the 3561 h required by the WRF-UCM in the same computing environment. Future research should focus on exploring the applicability of this approach to other urban areas with different climatic and urban characteristics, which could provide valuable insights for global urban heat mitigation efforts.

CRediT authorship contribution statement

JiHyun Kim: Writing – original draft, Methodology, Investigation, Formal analysis, Data curation, Conceptualization. **Suyeon Choi:** Writing – original draft, Software, Methodology, Investigation, Conceptualization. **Mahdi Panahi:** Writing – review & editing, Software, Data curation, Conceptualization. **Dan Li:** Writing – review & editing, Conceptualization. **Yeonjoo Kim:** Writing – review & editing, Supervision, Methodology, Funding acquisition.

Data statement

Land cover data from the Environmental Geographic Information Service of South Korea (https://egis.me.go.kr/) is available at https://zenodo.org/records/14550383. The land cover projection is from

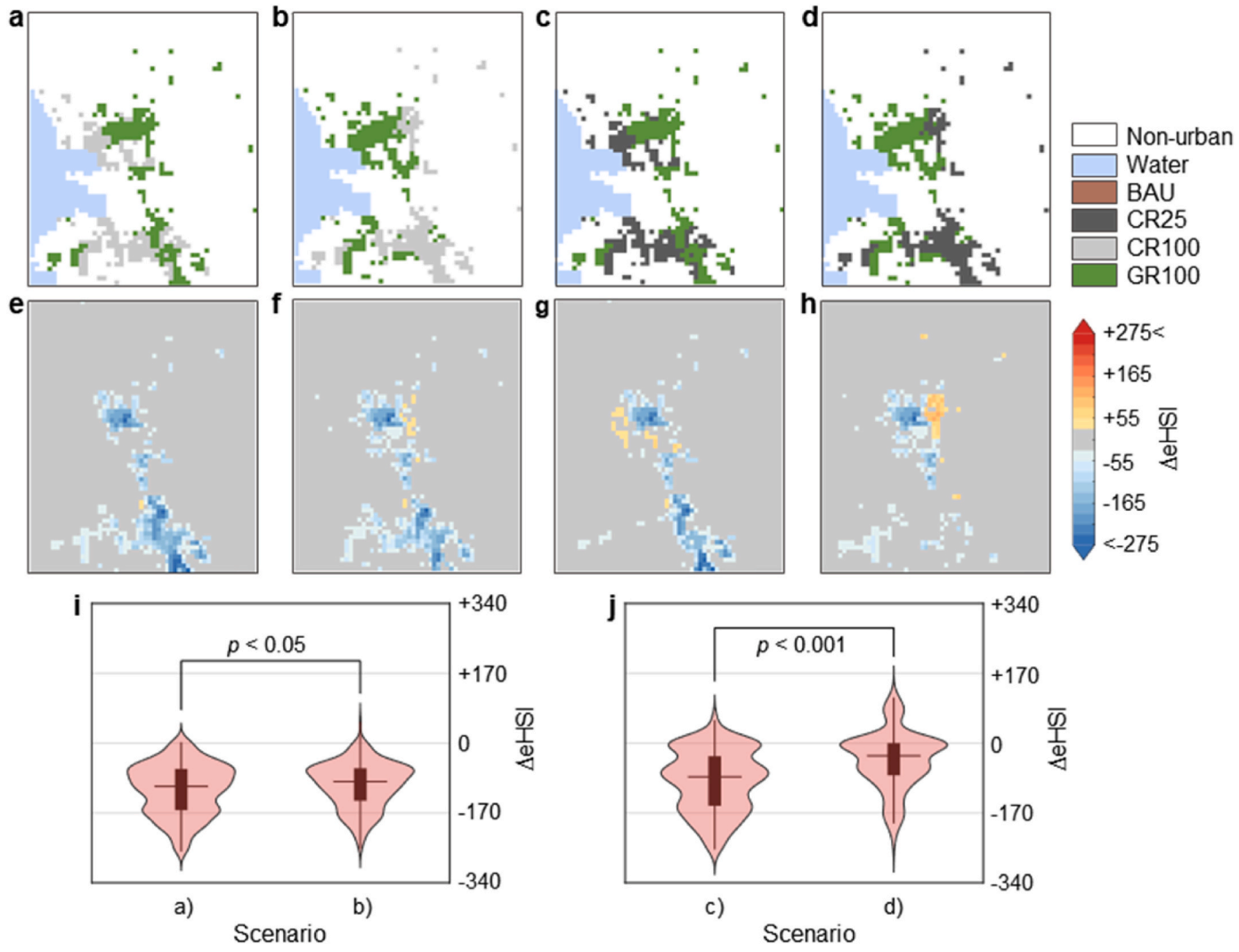

Fig. 8. Heat mitigation effects of green roof (GR) implementation strategies. (a–d) Two scenarios with contrasting spatial allocations but an identical composition, half of the area with 100 % GRs (GR100) and the rest with either 100 % cool roofs (CR100) or 25 % CRs (CR25). (e–h) Total effective heat stress index (eHSI) relative to the business-as-usual (BAU) scheme (ΔeHSI). (i–j) Violin plots showing the density distribution of ΔeHSI for each scenario and boxplots representing the 10th, 25th, 50th, 75th, and 90th percentiles (lower whisker, lower box edge, middle line, upper box edge, and upper whisker, respectively). Based on non-parametric Kruskal-Wallis tests, ΔeHSI differed significantly between the scenarios in (a) and (b) ($\chi^2 = 4.042$, $p < 0.05$) and between the scenarios in (c) and (d) ($\chi^2 = 57.188$, $p < 0.001$).

Chae et al. (2017). (https://www.nkis.re.kr/subject_view1.do?otpId=KEI00052847&otpSeq=0&popup=P). Observational data from the National Climate Data Portal of the Korea Meteorological Administration (https://data.kma.go.kr) are available at https://zenodo.org/records/14550383. Initial and boundary conditions for WRF-UCM implementation are available from Xu et al. (2021).

Declaration of competing interest

The authors declare that they have no known competing financial interests or personal relationships that could have appeared to influence the work reported in this paper.

Acknowledgements

This study was supported by National Research Foundation of Korea (NRF) grants funded by the Korean government (MSIT) (RS-2022-NR072388, RS-2024-00456724), and the Korea Environment Industry & Technology Institute (KEITI) through the R&D Programs for Innovative Flood Protection Technologies against Climate Crisis, and Water Management Program for Drought funded by the Korean Ministry of Environment (MOE) (RS-2023-00218873, RS-2023-00231944).

Appendix A. Supplementary data

Supplementary data to this article can be found online at https://doi.org/10.1016/j.jenvman.2025.125398.

Data availability

Data will be made available on request.

References

Abdi, M., Nahavandi, S., 2016. Multi-residual Networks: Improving the Speed and Accuracy of Residual Networks. https://doi.org/10.48550/arXiv.1609.05672.

Berardi, U., GhaffarianHoseini, AmirHosein, GhaffarianHoseini, Ali, 2014. State-of-the-art analysis of the environmental benefits of green roofs. Appl. Energy 115, 411–428. https://doi.org/10.1016/j.apenergy.2013.10.047.

Castleton, H.F., Stovin, V., Beck, S.B.M., Davison, J.B., 2010. Green roofs; building energy savings and the potential for retrofit. Energy Build. 42, 1582–1591. https://doi.org/10.1016/j.enbuild.2010.05.004.

Chae, Y., Joohyung, L., Hope, C., 2017. Economic analysis of climate change damage in Korea using SSP-RCP scenario matrix. Korea Environ. Ins. 2017–03, 1–170.
Chavan, M.M., Patil, Asawari, Dalvi, L., Patil, Ajinkya, 2015. Mini batch k-means clustering on large dataset. Int. J. Sci. Eng. Technol. Res. 4, 1356–1358.
Clinton, N., Gong, P., 2013. MODIS detected surface urban heat islands and sinks: global locations and controls. Remote Sens. Environ. 134, 294–304. https://doi.org/10.1016/j.rse.2013.03.008.
Ding, W., Chen, H., 2024. Investigating the microclimate impacts of blue–green space development in the urban–rural fringe using the WRF-UCM model. Urban Clim. 54, 101865. https://doi.org/10.1016/j.uclim.2024.101865.
Du, R., Song, J., Huang, X., Wang, Q., Zhang, C., Brousse, O., Chan, P.W., 2022. High-resolution regional modeling of urban moisture island: mechanisms and implications on thermal comfort. Build. Environ. 207, 108542. https://doi.org/10.1016/j.buildenv.2021.108542.
Fischer, E.M., Sippel, S., Knutti, R., 2021. Increasing probability of record-shattering climate extremes. Nat. Clim. Change 11, 689–695. https://doi.org/10.1038/s41558-021-01092-9.
Georgescu, M., 2015. Challenges associated with adaptation to future urban expansion. J. Clim. 28, 2544–2563. https://doi.org/10.1175/JCLI-D-14-00290.1.
Ghorbanzadeh, O., Shahabi, H., Crivellari, A., Homayouni, S., Blaschke, T., Ghamisi, P., 2022. Landslide detection using deep learning and object-based image analysis. Landslides 19, 929–939. https://doi.org/10.1007/s10346-021-01843-x.
Gunantara, N., 2018. A review of multi-objective optimization: methods and its applications. Cogent Eng. 5, 1502242.
Ha, K.-J., Seo, Y.-W., Yeo, J.-H., Timmermann, A., Chung, E.-S., Franzke, C.L.E., Chan, J. C.L., Yeh, S.-W., Ting, M., 2022. Dynamics and characteristics of dry and moist heatwaves over East Asia. npj Clim. Atmos. Sci. 5, 49. https://doi.org/10.1038/s41612-022-00272-4.
Hong, S.-Y., Dudhia, J., Chen, S.-H., 2004. A revised approach to ice microphysical processes for the bulk parameterization of clouds and precipitation. Mon. Weather Rev. 132, 103–120.
Hong, Y., Hsu, K., Moradkhani, H., Sorooshian, S., 2006. Uncertainty quantification of satellite precipitation estimation and Monte Carlo assessment of the error propagation into hydrologic response. Water Resour. Res. 42.
Huang, K., Li, X., Liu, X., Seto, K.C., 2019. Projecting global urban land expansion and heat island intensification through 2050. Environ. Res. Lett. 14. https://doi.org/10.1088/1748-9326/ab4b71.
Huang, W.T.K., Masselot, P., Bou-Zeid, E., Fatichi, S., Paschalis, A., Sun, T., Gasparrini, A., Manoli, G., 2023. Economic valuation of temperature-related mortality attributed to urban heat islands in European cities. Nat. Commun. 14, 7438. https://doi.org/10.1038/s41467-023-43135-z.
Jiang, S., Lee, X., Wang, J., Wang, K., 2019. Amplified urban heat islands during heat wave periods. J. Geophys. Res. Atmos. 124, 7797–7812. https://doi.org/10.1029/2018JD030230.
Jiménez, P.A., Dudhia, J., González-Rouco, J.F., Navarro, J., Montávez, J.P., García-Bustamante, E., 2012. A revised scheme for the WRF surface layer formulation. Mon. Weather Rev. 140, 898–918.
Johnson, J.M., Khoshgoftaar, T.M., 2019. Survey on deep learning with class imbalance. J. Big Data 6, 27. https://doi.org/10.1186/s40537-019-0192-5.
Kain, J.S., Fritsch, J.M., 1990. A one-dimensional entraining/detraining plume model and its application in convective parameterization. J. Atmos. Sci. 47, 2784–2802.
Kusaka, H., Kimura, F., 2004. Thermal effects of urban canyon structure on the nocturnal heat island: numerical experiment using a mesoscale model coupled with an urban canopy model. J. Appl. Meteorol. 43, 1899–1910. https://doi.org/10.1175/JAM2169.1.
Kusaka, H., Kondo, H., Kikegawa, Y., Kimura, F., 2001. A simple single-layer urban canopy model for atmospheric models: comparison with multi-layer and slab models. Boundary-Layer Meteorol. 101, 329–358.
Laloy, E., Jacques, D., 2019. Emulation of CPU-demanding reactive transport models: a comparison of Gaussian processes, polynomial chaos expansion, and deep neural networks. Comput. Geosci. 23, 1193–1215. https://doi.org/10.1007/s10596-019-09875-y.
LeCun, Y., Bengio, Y., Hinton, G., 2015. Deep learning. Nature 521, 436–444. https://doi.org/10.1038/nature14539.
Li, D., Bou-Zeid, E., Oppenheimer, M., 2014. The effectiveness of cool and green roofs as urban heat island mitigation strategies. Environ. Res. Lett. 9, 055002. https://doi.org/10.1088/1748-9326/9/5/055002.
Li, P., Wang, Z.-H., 2020. Modeling carbon dioxide exchange in a single-layer urban canopy model. Build. Environ. 184, 107243. https://doi.org/10.1016/j.buildenv.2020.107243.
Li, P., Xu, T., Wei, S., Wang, Z.H., 2022. Multi-objective optimization of urban environmental system design using machine learning. Comput. Environ. Urban Syst. 94, 101796. https://doi.org/10.1016/j.compenvurbsys.2022.101796.
Li, Y., Svenning, J.-C., Zhou, W., Zhu, K., Abrams, J.F., Lenton, T.M., Ripple, W.J., Yu, Z., Teng, S.N., Dunn, R.R., Xu, C., 2024. Green spaces provide substantial but unequal urban cooling globally. Nat. Commun. 15, 7108. https://doi.org/10.1038/s41467-024-51355-0.
Liu, S., Zhang, J., Wang, K., Wu, X., Chen, W., Liang, S., Zhang, Y., Fu, S., 2023. Structural indicator synergy for mitigating extreme urban heat island effects in industrial city: simulation and verification based on machine learning. Ecol. Indic. 157, 111216. https://doi.org/10.1016/j.ecolind.2023.111216.
Liu, S., Zhang, Jianjun, Li, J., Li, Y., Zhang, Jie, Wu, X., 2021. Simulating and mitigating extreme urban heat island effects in a factory area based on machine learning. Build. Environ. 202, 108051. https://doi.org/10.1016/j.buildenv.2021.108051.
Lloyd, S., 1982. Least squares quantization in PCM. IEEE Trans. Inf. Theor. 28, 129–137. https://doi.org/10.1109/TIT.1982.1056489.
Manso, M., Teotónio, I., Silva, C.M., Cruz, C.O., 2021. Green roof and green wall benefits and costs: a review of the quantitative evidence. Renew. Sustain. Energy Rev. 135. https://doi.org/10.1016/j.rser.2020.110111.
Mlawer, E.J., Taubman, S.J., Brown, P.D., Iacono, M.J., Clough, S.A., 1997. Radiative transfer for inhomogeneous atmospheres: RRTM, a validated correlated-k model for the longwave. J. Geophys. Res. Atmos. 102, 16663–16682.
Nainggolan, R., Perangin-Angin, R., Simarmata, E., Tarigan, A.F., 2019. Improved the performance of the K-means cluster using the sum of squared error (SSE) optimized by using the elbow method. J. Phys. Conf. Ser. 1361. https://doi.org/10.1088/1742-6596/1361/1/012015.
Ngatchou, P., Zarei, A., El-Sharkawi, A., 2005. Pareto multi objective optimization. In: Proceedings of the 13th International Conference on, Intelligent Systems Application to Power Systems. IEEE, pp. 84–91.
Northridge, M.E., Sclar, E., 2003. A joint urban planning and public health framework: contributions to health impact assessment. Am. J. Publ. Health 93, 118–121. https://doi.org/10.2105/AJPH.93.1.118.
Oke, T.R., 1973. City size and the urban heat island. Atmos. Environ. 7, 769–779. https://doi.org/10.1016/0004-6981(73)90140-6.
Peng, S., Piao, S., Ciais, P., Friedlingstein, P., Ottle, C., Bréon, F.-M., Nan, H., Zhou, L., Myneni, R.B., 2012. Surface urban heat island across 419 global big cities. Environ. Sci. Technol. 46, 696–703. https://doi.org/10.1021/es2030438.
Rasp, S., Pritchard, M.S., Gentine, P., 2018. Deep learning to represent subgrid processes in climate models. Proc. Natl. Acad. Sci. 115, 9684–9689. https://doi.org/10.1073/pnas.1810286115.
Rawat, M., Singh, R.N., 2022. A study on the comparative review of cool roof thermal performance in various regions. Energy Built Environ 3, 327–347. https://doi.org/10.1016/j.enbenv.2021.03.001.
Rothfusz, L.P., 1990. The heat index equation (or, more than you ever wanted to know about heat index). National Weather Service (NWS). Technical Attachment (SR/SSD 90-23, 23–90.
Schwarz, K., Fragkias, M., Boone, C.G., Zhou, W., McHale, M., Grove, J.M., O'Neil-Dunne, J., McFadden, J.P., Buckley, G.L., Childers, D., 2015. Trees grow on money: urban tree canopy cover and environmental justice. PLoS One 10, e0122051.
Sculley, D., 2010. Web-scale k-means clustering. In: Proceedings of the 19th International Conference on World Wide Web, pp. 1177–1178.
Sharma, A., Conry, P., Fernando, H.J.S., Hamlet, A.F., Hellmann, J.J., Chen, F., 2016. Green and cool roofs to mitigate urban heat island effects in the Chicago metropolitan area: evaluation with a regional climate model. Environ. Res. Lett. 11, 064004. https://doi.org/10.1088/1748-9326/11/6/064004.
Skamarock, W.C., Klemp, J.B., Dudhia, J., Gill, D.O., Barker, D.M., Duda, M.G., Huang, X.-Y., Wang, W., Powers, J.G., 2008. A description of the advanced research WRF version 3. NCAR Tech. note 475, 113.
Skamarock, W.C., Klemp, J.B., Dudhia, J., Gill, D.O., Liu, Z., Berner, J., Huang, X.Y., 2021. A description of the advanced research WRF model version 4.3 (No. NCAR/TN-556+ STR). https://doi.org/10.5065/1dfh-6p97.
Sproul, J., Wan, M.P., Mandel, B.H., Rosenfeld, A.H., 2014. Economic comparison of white, green, and black flat roofs in the United States. Energy Build. 71, 20–27. https://doi.org/10.1016/j.enbuild.2013.11.058.
Srivastava, N., Hinton, G., Krizhevsky, A., Sutskever, I., Salakhutdinov, R., 2014. Dropout: a simple way to prevent neural networks from overfitting. J. Mach. Learn. Res. 15, 1929–1958.
Syakur, M.A., Khotimah, B.K., Rochman, E.M.S., Satoto, B.D., 2018. Integration K-means clustering method and elbow method for identification of the best customer profile cluster. IOP Conf. Ser. Mater. Sci. Eng. 336. https://doi.org/10.1088/1757-899X/336/1/012017.
Tewari, M., Chen, F., Wang, W., Dudhia, J., LeMone, M.A., Mitchell, K., 2004. Implementation and verification of the unified NOAH land surface model in the WRF model. In: 20th Conference on Weather Analysis and Forecasting/16th Conference on Numerical Weather Prediction, pp. 11–15. Seattle, WA.
Vahmani, P., Hogue, T.S., 2015. Urban irrigation effects on WRF-UCM summertime forecast skill over the Los Angeles metropolitan area. J. Geophys. Res. Atmos. 120, 9869–9881. https://doi.org/10.1002/2015JD023239.
Wang, X., Li, H., Sodoudi, S., 2022. The effectiveness of cool and green roofs in mitigating urban heat island and improving human thermal comfort. Build. Environ. 217, 109082. https://doi.org/10.1016/j.buildenv.2022.109082.
Wang, X., Wang, T., Guo, H., Liu, D., Zhao, Y., Zhang, T., Liu, Q., Piao, S., 2018. Disentangling the mechanisms behind winter snow impact on vegetation activity in northern ecosystems. Glob. Change Biol. 24, 1651–1662. https://doi.org/10.1111/gcb.13930.
Wang, Y., Di Sabatino, S., Martilli, A., Li, Y., Wong, M.S., Gutiérrez, E., Chan, P.W., 2017. Impact of land surface heterogeneity on urban heat island circulation and sea-land breeze circulation in Hong Kong. J. Geophys. Res. Atmos. 122, 4332–4352. https://doi.org/10.1002/2017JD026702.
Xu, Z., Han, Y., Tam, C.-Y., Yang, Z.-L., Fu, C., 2021. Bias-corrected CMIP6 global dataset for dynamical downscaling of the historical and future climate (1979–2100). Sci. Data 8, 293. https://doi.org/10.1038/s41597-021-01079-3.
Yu, S., Ma, J., 2021. Deep learning for geophysics: current and future trends. Rev. Geophys. 59, e2021RG000742. https://doi.org/10.1029/2021RG000742.
Zhong, T., Zhang, N., Lv, M., 2021. A numerical study of the urban green roof and cool roof strategies' effects on boundary layer meteorology and ozone air quality in a

megacity. Atmos. Environ. 264, 118702. https://doi.org/10.1016/j.atmosenv.2021.118702.
Zhong, Z., Sun, A.Y., Yang, Q., Ouyang, Q., 2019. A deep learning approach to anomaly detection in geological carbon sequestration sites using pressure measurements. J. Hydrol. 573, 885–894. https://doi.org/10.1016/j.jhydrol.2019.04.015.
Zonato, A., Martilli, A., Gutierrez, E., Chen, F., He, C., Barlage, M., Zardi, D., Giovannini, L., 2021. Exploring the effects of rooftop mitigation strategies on urban temperatures and energy consumption. J. Geophys. Res. Atmos. 126. https://doi.org/10.1029/2021JD035002.